Nonequilibrium electron transport in a hybrid superconductor–normal metal entangler in a dissipative environment

Vladimir Bubanja,[1,2] Mayumi Yamamoto,[3] and Shuichi Iwabuchi[3]
[1]*Measurement Standards Laboratory of New Zealand, Callaghan Innovation, P.O. Box 31310, Lower Hutt 5040, Wellington, New Zealand*
[2]*The Dodd-Walls Centre for Photonic and Quantum Technologies, University of Otago, 730 Cumberland Street, Dunedin 9016, New Zealand*
[3]*Department of Physics, Nara Women's University, Kitauoya-Nishimachi, Nara 630-8506, Japan*
(Received 9 May 2016; revised manuscript received 4 November 2016; published 28 November 2016)

We consider a three-terminal Cooper-pair splitting device with a superconducting electrode tunnel coupled to two normal metal electrodes. We employ the Nambu-Gor'kov and Schwinger-Keldysh formalisms to describe the nonequilibrium transport properties of the device for arbitrary transmissions of the barriers and for a general electromagnetic environment. We derive the analytic expressions for the current and the nonlocal differential conductance, and analyze the limits of clean and dirty superconductivity.

DOI: 10.1103/PhysRevB.94.184515

I. INTRODUCTION

The controlled production and detection of entangled pairs is essential for quantum information processing. Conventional Bardeen-Cooper-Schrieffer (BCS) superconductors have been identified as a potential source of entangled particles since Cooper pairs in these materials form the spin singlet states. Various mechanisms were considered that would favor splitting of a pair of electrons while it is extracted from a superconductor. For instance, studies have been reported that utilize Coulomb repulsion of electrons in quantum dots [1], spin-charge separation in Tomonaga-Luttinger liquids in one-dimensional quantum wires [2], or the relativistic band structure with proximity induced superconductivity in graphene nanoribbons [3]. Recent proposals were based on helicity conservation of the edge states in quantum spin Hall insulators [4], or the antiferromagnetic magnetization in silicene forming a spin-valley topological insulator [5]. Controlling and maximizing the splitting process is required for efficient entanglement detection. This latter step could be achieved by testing the violation of Bell's inequalities [6], determining concurrence [7], or entanglement witnessing [8]. Other detection mechanisms that were put forward employed the entanglement of formation [9], microwave spectroscopy [10], or a toolkit developed for spin qubits [11].

In this paper we consider a device, schematically represented in Fig. 1, consisting of a grounded superconductor, coupled to two voltage-biased normal metal leads [12–15]. The dynamical Coulomb blockade effect caused by the impedance of the normal metal leads facilitates the splitting of the Cooper pairs tunneling out of the superconducting electrode and creating mobile and nonlocal spin-entangled electrons in the normal metal leads. We develop the theory that describes the nonequilibrium electron transport in the system to infinite order in the tunnel Hamiltonian, and obtain results for the current and the nonlocal differential conductance. Measurements of nonlocal resistance as well as cross correlations in such a setup showed evidence of nonlocal entanglement [16]. Our theory highlights features of the nonlocal transport that are possible to further test experimentally.

Within noninteracting theory, the contributions of crossed Andreev reflection (CAR) and elastic cotunneling (EC) processes to the nonlocal differential conductance cancel each other in the lowest order of perturbation in the tunnel Hamiltonian [12]. A difference in contributions between these two processes emerges with increasing transmissions of the barriers, that is, by taking into account the higher order perturbation terms [17–19]. This difference can also result in the lowest order in the tunnel Hamiltonian when electron-electron interactions are taken into account. Either CAR or EC can be suppressed, depending on the symmetry of the electromagnetic modes propagating in the superconductor, which in turn results from the device geometry [20]. To make the problem mathematically tractable, in studies that include both the perturbation in the tunnel Hamiltonian to infinite order and the electron-electron interactions, it is typically assumed that this interaction is weak [21–24]. In our approach, we include the tunnel Hamiltonian to infinite order and allow an arbitrary strength of the electron-electron interactions by performing the partial resummation of the associated diagrams.

In addition to applications in quantum information science, hybrid superconductor–normal metal devices have recently attracted attention also in studies involving metrology applications such as the quantum standard of the electric current [25]. These devices are based on the transfer of one electron through the circuit per period of the driving gate voltage source. However, aside from the desired single electron tunneling, higher order processes involving simultaneous tunneling of several electrons, which we study in this paper, have to be taken into account in considerations regarding the ultimate accuracy achievable by such devices [26]. Our results illuminate the properties of electron dynamics also in these hybrid systems.

The paper is organized as follows. In Sec. II, we introduce the formalism and obtain the analytic result for the current in our device to all orders in the tunnel Hamiltonian. This is used to derive the expressions for the nonlocal differential conductance in the limits of clean and dirty superconductors. We present the conclusions in Sec. III. The expressions for the local and nonlocal bare Green's functions in the

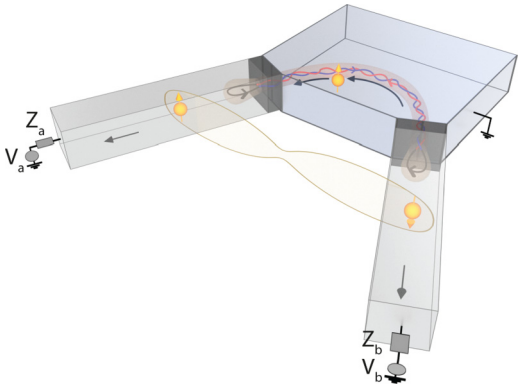

FIG. 1. Schematic geometry of the device under consideration: a bulk BCS superconductor is coupled to two normal metal leads. Voltages between the leads (with impedances Z_a and Z_b) and the superconductor are V_a and V_b. We consider the clean and dirty limits of the superconductor. In the dirty limit, we average over disorder the products of retarded and advanced Green's functions corresponding to crossed-Andreev reflection (pair splitting) and elastic cotunneling processes (between the normal metal electrodes); these Green's functions are represented by the red and blue lines inside the superconductor.

superconducting and normal metal electrodes are presented in the Appendices.

II. FORMALISM AND RESULTS

In order to develop a description of our system that will enable quantitative analysis, our approach starts with the following Hamiltonian:

$$H = H_0 + H_T, \tag{1}$$

where the unperturbed part H_0, describing the uncoupled normal metal (a and b) and superconducting (c) electrodes, as well as the electromagnetic environment (Z_a, Z_b), is given by

$$\begin{aligned} H_0 = \frac{1}{2} \sum_{\substack{\mathbf{k},\sigma \\ f\in\{a,b,c\}}} & \boldsymbol{\Psi}_f^\dagger(\mathbf{k},\sigma) \\ & \times \left[\xi_{\mathbf{k}}^{(f)}\boldsymbol{\tau}_3 - \mathrm{sgn}(\sigma)(\Delta\boldsymbol{\tau}_+ + \Delta^*\boldsymbol{\tau}_-)\delta_{f,c}\right]\boldsymbol{\Psi}_f(\mathbf{k},\sigma) \\ & + \sum_{\mathbf{q},\alpha\in\{a,b\}} \hbar\omega_{\mathbf{q}}^{(\alpha)} b_{\mathbf{q}}^{(\alpha)\dagger} b_{\mathbf{q}}^{(\alpha)}, \end{aligned} \tag{2}$$

where $\mathrm{sgn}(\uparrow / \downarrow) = +1/-1$, and Δ is the superconducting order parameter. The Pauli matrices $\boldsymbol{\tau}_i$ are given by

$$\begin{aligned} \boldsymbol{\tau}_1 &= \begin{pmatrix} 0 & 1 \\ 1 & 0 \end{pmatrix}, \quad \boldsymbol{\tau}_2 = \begin{pmatrix} 0 & -i \\ i & 0 \end{pmatrix}, \\ \boldsymbol{\tau}_3 &= \begin{pmatrix} 1 & 0 \\ 0 & -1 \end{pmatrix}, \quad \boldsymbol{\tau}_\pm = \tfrac{1}{2}(\boldsymbol{\tau}_1 \pm i\boldsymbol{\tau}_2). \end{aligned} \tag{3}$$

The Nambu-Gor'kov spinor $\boldsymbol{\Psi}_f(\mathbf{k},\sigma)$, appearing in Eq. (2), is given by

$$\boldsymbol{\Psi}_f(\mathbf{k},\sigma) = \begin{pmatrix} f_{\mathbf{k},\sigma} \\ f_{-\mathbf{k},-\sigma}^\dagger \end{pmatrix}. \tag{4}$$

The tunnel Hamiltonian in Eq. (1) is treated as a perturbation and is given by

$$\begin{aligned} H_T &= \sum_{\substack{\mathbf{k},\mathbf{k}',\sigma \\ \alpha=a,b}} \boldsymbol{\Psi}_c^\dagger(\mathbf{k},\sigma)\mathbf{T}^{(\alpha)}(\mathbf{k},\mathbf{k}')\boldsymbol{\Psi}_\alpha(\mathbf{k}',\sigma), \\ \mathbf{T}^{(\alpha)}(\mathbf{k},\mathbf{k}') &= \begin{pmatrix} T_{\mathbf{k},\mathbf{k}'}^{(\alpha)} e^{i\phi_\alpha} & 0 \\ 0 & -T_{\mathbf{k},\mathbf{k}'}^{(\alpha)*} e^{-i\phi_\alpha} \end{pmatrix}. \end{aligned} \tag{5}$$

The phase ϕ_α, appearing in (5), corresponds to the electromagnetic environment in the normal metal electrode α, and consists of the classical part due to the ideal voltage source, and the quantum part due to the circuit impedance, $\phi_\alpha(t) = \frac{e}{\hbar}V_\alpha(t) + \tilde{\phi}_\alpha(t)$ [27]. The latter part can be expressed as a linear combination of Bose operators $\{b_{\mathbf{q}}^{(\alpha)}, b_{\mathbf{q}}^{(\alpha)\dagger}\}$ corresponding to the normal modes of the environment.

In order to consider the current through the system to all orders in the tunnel Hamiltonian, we introduce the following Green's functions in the Keldysh ($\check{}$)⊗Nambu ($\hat{}$) space,

$$\begin{aligned} \check{\mathbf{G}}_{fg}(\mathbf{k},\sigma,t;\mathbf{k}',\sigma',t') &= -i\langle \mathcal{T}_c \boldsymbol{\Psi}_f((\mathbf{k},\sigma,t)\boldsymbol{\Psi}_g^\dagger((\mathbf{k}',\sigma',t')\rangle \\ &= \begin{pmatrix} \hat{\mathbf{G}}_{fg}^{--} & \hat{\mathbf{G}}_{fg}^{<} \\ \hat{\mathbf{G}}_{fg}^{>} & \hat{\mathbf{G}}_{fg}^{++} \end{pmatrix}, \end{aligned} \tag{6}$$

where $f,g \in \{a,b,c\}$, and $\mathcal{T}_c$ is the time ordering operator along the Schwinger-Keldysh contour. Each of the blocks on the right-hand side of Eq. (6) is a 2×2 matrix in the Nambu space. The above Green's functions satisfy the Dyson equation,

$$\check{\mathbf{G}} = \check{\mathbf{g}} + \check{\mathbf{g}} \boxtimes \check{\boldsymbol{\Sigma}} \boxtimes \check{\mathbf{G}}, \tag{7}$$

where $\boxtimes$ stands for the matrix multiplication over electrode labels and convolution over the spacial and contour time variables. After performing the unitary transformations, $\check{\mathbf{G}} \to \bar{\mathbf{G}} = \mathbf{R}\boldsymbol{\tau}_3\check{\mathbf{G}}\mathbf{R}^{-1}$, $\check{\boldsymbol{\Sigma}} \to \bar{\boldsymbol{\Sigma}} = \mathbf{R}\check{\boldsymbol{\Sigma}}\boldsymbol{\tau}_3\mathbf{R}^{-1}$, where $\mathbf{R} = \frac{1}{\sqrt{2}}(\boldsymbol{\tau}_0 - i\boldsymbol{\tau}_2)$, with $\boldsymbol{\tau}_0$ being the identity matrix, the Green's functions and the self-energy matrices obtain the triangular form:

$$\bar{\mathbf{G}} = \begin{pmatrix} \hat{\mathbf{G}}^R & \hat{\mathbf{G}}^K \\ \mathbf{0} & \hat{\mathbf{G}}^A \end{pmatrix}, \quad \bar{\boldsymbol{\Sigma}} = \begin{pmatrix} \hat{\boldsymbol{\Sigma}}^R & \hat{\boldsymbol{\Sigma}}^K \\ \mathbf{0} & \hat{\boldsymbol{\Sigma}}^A \end{pmatrix}. \tag{8}$$

The current through the electrode $\alpha = (a,b)$, which is the average of the current operator $\mathcal{I}_\sigma^{(\alpha)}(t) = \frac{ie}{\hbar}[N_\sigma^{(\alpha)}, H_T(t)]$, where $N_\sigma^{(\alpha)} = \sum_{\mathbf{k}} \alpha_{\mathbf{k},\sigma}^\dagger \alpha_{\mathbf{k},\sigma}$, can be expressed in terms of the above Green's functions as

$$I_\sigma^{(\alpha)}(t) = -\frac{2e}{\hbar}\mathrm{Re}\left\{\sum_{\mathbf{k},\mathbf{k}'} T_{\mathbf{k},\mathbf{k}'}^{(\alpha)*} G_{c\tilde{\alpha}11}^{<}(\mathbf{k},\sigma,t;\mathbf{k}',\sigma,t)\right\}, \tag{9}$$

where we introduce the operator $\tilde{\alpha}_{\mathbf{k},\sigma}(t) \equiv e^{i\phi_\alpha(t)}\alpha_{\mathbf{k},\sigma}(t)$. The mixed ($c\tilde{\alpha}$) Green's function, appearing in the above equation, is obtained from Eq. (6), by considering the "11" component in the Nambu space of $\hat{\mathbf{G}}_{c\tilde{\alpha}}(\mathbf{k},\sigma,t;\mathbf{k}',\sigma',t')$. In the interaction picture this Green's function takes the form $\check{\mathbf{G}}_{c\tilde{\alpha}11}(\mathbf{k},\sigma,t;\mathbf{k}',\sigma',t') = \langle \mathcal{T}_c c_{\mathbf{k},\sigma}(t)\tilde{\alpha}_{\mathbf{k}',\sigma'}^\dagger(t')S_c\rangle$, where $S_c = \mathcal{T}_c \exp[-\frac{i}{\hbar}\int_c dt H_T(t)]$ is the evolution operator along the Schwinger-Keldysh contour. In the diagrammatic language, the lesser component of this Green's function can be represented by the sum of all topologically distinct diagrams, an example of which is shown in Fig. 2. We take into

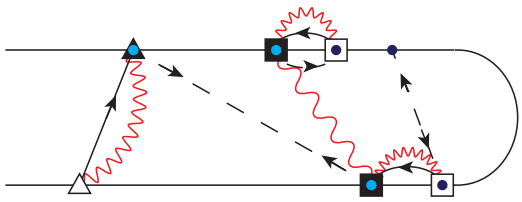

FIG. 2. An example of a diagram obtained in the expansion of $\check{\mathbf{G}}_{c\tilde{a}11}$. The upper (lower) horizontal line corresponds to the "−" ("+") branch of the Schwinger-Keldysh contour. The empty (filled) triangles represent the creation (annihilation) operators in the normal metal electrode a; analogously squares represent the operators for the electrode b. Light (dark) blue dots correspond to the creation (annihilation) operators for the electrons in the supeconducting electrode. Wick contractions are represented by solid lines connecting the operators of the same normal metal electrode, and by dashed lines connecting superconducting electrode operators. Wiggly lines (red) represent phase-phase correlation functions corresponding to the electromagnetic environment. While we show only a couple of such lines, every pair of shapes (triangles or squares) corresponding to the same normal metal electrode is joined by such lines.

account only the dominant boson interactions by dressing the solid lines representing the contractions between creation and annihilation operators of the same normal metal electrode. By further employing the Langreth theorem for analytic continuation one can transition to real time integrals, and after performing the Fourier transform, one can obtain

$$I_\sigma^{(\alpha)} = \frac{e}{\hbar^3}|t^{(\alpha)}|^2\int_{-\infty}^{\infty}\frac{d\epsilon}{2\pi}\big[G^<_{cc11}(\mathbf{x}_\alpha,\mathbf{x}_\alpha;\epsilon)g^>_{\tilde{a}\tilde{a}11}(\mathbf{x}_\alpha,\mathbf{x}_\alpha;\epsilon) - G^>_{cc11}(\mathbf{x}_\alpha,\mathbf{x}_\alpha;\epsilon)g^<_{\tilde{a}\tilde{a}11}(\mathbf{x}_\alpha,\mathbf{x}_\alpha;\epsilon)\big], \tag{10}$$

where we introduce the Green's functions in the coordinate representation,

$$\check{\mathbf{G}}_{fg11}(\mathbf{x}_\alpha,\mathbf{x}_\beta;\epsilon) = \frac{1}{\Omega_c}\sum_{\mathbf{k},\mathbf{k}'}e^{i\mathbf{k}\mathbf{r}_\alpha}\check{\mathbf{G}}_{fg11}(\mathbf{k},\sigma,\mathbf{k}',\sigma';\epsilon)e^{-i\mathbf{k}'\mathbf{r}_\beta}, \tag{11}$$

where $\mathbf{x}_\alpha = (\mathbf{r}_\alpha,\sigma)$, $\mathbf{x}_\beta = (\mathbf{r}_\beta,\sigma')$, and Ω_c is the volume of the superconducting electrode. Coordinate representation of the Green's functions in the rotated Keldysh space ($\bar{\mathbf{G}}_{fg11}$) are defined analogously. In deriving (10), we assumed the point contact geometry of the junctions, that is, in the coordinate representation the tunnel matrix elements take the form $T^{(\alpha)}(\mathbf{r}_1,\mathbf{r}_2) = t^{(\alpha)}\delta(\mathbf{r}_1-\mathbf{r}_\alpha)\delta(\mathbf{r}_2-\mathbf{r}_\alpha)$, for $\mathbf{r}_1$ and $\mathbf{r}_2$ belonging to the electrodes on the left- and the right-hand sides of the junction located at $\mathbf{r}_\alpha$. The elements of the superconductor lesser and greater Green's functions, appearing in (10) are obtained from the Keldysh equation,

$$\hat{\mathbf{G}}^{\gtrless}_{cc}(\mathbf{x}_a,\mathbf{x}_a;\epsilon) = \sum_{\alpha,\beta=a,b}\Big[\boldsymbol{\tau}_0\delta_{\alpha,a} + \hat{\mathbf{G}}^R_{c\tilde{\alpha}}(\mathbf{x}_a,\mathbf{x}_\alpha;\epsilon)\hat{\boldsymbol{\Sigma}}^R_{\alpha c}\Big]\hat{\mathbf{g}}^{\gtrless}_{c\tilde{c}}(\mathbf{x}_\alpha,\mathbf{x}_\beta;\epsilon)\big[\boldsymbol{\tau}_0\delta_{\beta,a} + \hat{\boldsymbol{\Sigma}}^A_{c\beta}\hat{\mathbf{G}}^A_{\tilde{\beta}c}(\mathbf{x}_\beta,\mathbf{x}_a;\epsilon)\big] + \sum_{\beta=a,b}\hat{\mathbf{G}}^R_{cc}(\mathbf{x}_a,\mathbf{x}_\beta;\epsilon)\hat{\boldsymbol{\Sigma}}^R_{c\beta}\hat{\mathbf{g}}^{\gtrless}_{\tilde{\beta}\tilde{\beta}}(\mathbf{x}_\beta,\mathbf{x}_\beta;\epsilon)\hat{\boldsymbol{\Sigma}}^A_{\beta c}\hat{\mathbf{G}}^A_{\tilde{c}c}(\mathbf{x}_\beta,\mathbf{x}_a;\epsilon), \tag{12}$$

and analogously for the junction located at $\mathbf{r}_b$. The above retarded and advanced Green's functions are obtained from the Dyson equation (7), and the self-energy matrices are given by

$$\hat{\boldsymbol{\Sigma}}^R_{\alpha c} = \hat{\boldsymbol{\Sigma}}^A_{\alpha c} = \begin{pmatrix}\tilde{t}^{(\alpha)} & 0\\ 0 & -\tilde{t}^{(\alpha)*}\end{pmatrix} = \hat{\boldsymbol{\Sigma}}^{R*}_{c\alpha} = \hat{\boldsymbol{\Sigma}}^{A*}_{c\alpha}, \tag{13}$$

where $\tilde{t}^{(\alpha)} = t^{(\alpha)}/\hbar$. By substituting the expressions for $G^{\gtrless}_{cc11}(\mathbf{x}_\alpha,\mathbf{x}_\alpha;\epsilon)$, obtained from (12), into Eq. (10), we get

$$\begin{aligned}
I_\sigma^{(a)} = \frac{e}{\hbar^3}|t^{(a)}|^2\int_{-\infty}^{\infty}\frac{d\epsilon}{2\pi}\Bigg\{&\sum_{\mu,\nu=a,b}\Big(\big\{\big[1+\tilde{t}^{(a)*}G^R_{c\tilde{a}11}(\mathbf{x}_a,\mathbf{x}_a;\epsilon)\big]\delta_{\mu,a} + \tilde{t}^{(b)*}G^R_{c\tilde{b}11}(\mathbf{x}_a,\mathbf{x}_b;\epsilon)\delta_{\mu,b}\big\}\\
&\times\big\{\big[1+\tilde{t}^{(a)}G^A_{\tilde{a}c11}(\mathbf{x}_a,\mathbf{x}_a;\epsilon)\big]\delta_{\nu,a} + \tilde{t}^{(b)}G^A_{\tilde{b}c11}(\mathbf{x}_b,\mathbf{x}_a;\epsilon)\delta_{\nu,b}\big\}\\
&\times\big[g^<_{cc11}(\mathbf{x}_\mu,\mathbf{x}_\nu;\epsilon)g^>_{\tilde{a}\tilde{a}11}(\mathbf{x}_a,\mathbf{x}_a;\epsilon) - g^>_{cc11}(\mathbf{x}_\mu,\mathbf{x}_\nu;\epsilon)g^<_{\tilde{a}\tilde{a}11}(\mathbf{x}_a,\mathbf{x}_a;\epsilon)\big]\\
&-2\mathrm{Re}\big\{\big[\delta_{\mu,a}+\tilde{t}^{(\mu)*}G^R_{c\tilde{\mu}11}(\mathbf{x}_a,\mathbf{x}_\mu;\epsilon)\big]\tilde{t}^{(\nu)*}G^A_{\tilde{\nu}c21}(\mathbf{x}_\nu,\mathbf{x}_a;\epsilon)\big\}\\
&\times\big[g^<_{cc12}(\mathbf{x}_\mu,\mathbf{x}_\nu;\epsilon)g^>_{\tilde{a}\tilde{a}11}(\mathbf{x}_a,\mathbf{x}_a;\epsilon) - g^>_{cc12}(\mathbf{x}_\mu,\mathbf{x}_\nu;\epsilon)g^<_{\tilde{a}\tilde{a}11}(\mathbf{x}_a,\mathbf{x}_a;\epsilon)\big]\\
&+\tilde{t}^{(\mu)}\tilde{t}^{(\nu)*}G^R_{c\tilde{\mu}12}(\mathbf{x}_a,\mathbf{x}_\mu;\epsilon)G^A_{\tilde{\nu}c21}(\mathbf{x}_\nu,\mathbf{x}_a;\epsilon)\\
&\times\big[g^<_{cc22}(\mathbf{x}_\mu,\mathbf{x}_\nu;\epsilon)g^>_{\tilde{a}\tilde{a}11}(\mathbf{x}_a,\mathbf{x}_a;\epsilon) - g^>_{cc22}(\mathbf{x}_\mu,\mathbf{x}_\nu;\epsilon)g^<_{\tilde{a}\tilde{a}11}(\mathbf{x}_a,\mathbf{x}_a;\epsilon)\big]\Big)\\
&+\sum_{\substack{\mu=a,b\\ i=1,2}}\big|\tilde{t}^{(\mu)}G^R_{cc1i}(\mathbf{x}_a,\mathbf{x}_\mu;\epsilon)\big|^2\big[g^<_{\tilde{\mu}\tilde{\mu}ii}(\mathbf{x}_\mu,\mathbf{x}_\mu;\epsilon)g^>_{\tilde{a}\tilde{a}11}(\mathbf{x}_a,\mathbf{x}_a;\epsilon) - g^>_{\tilde{\mu}\tilde{\mu}ii}(\mathbf{x}_\mu,\mathbf{x}_\mu;\epsilon)g^<_{\tilde{a}\tilde{a}11}(\mathbf{x}_a,\mathbf{x}_a;\epsilon)\big]\Bigg\}.
\end{aligned} \tag{14}$$

The above expression enables calculations of the current to all orders in the tunnel Hamiltonian and for arbitrary temperature and voltage, as well as the circuit impedance. The approximation of electron-electron interactions dressing the normal metal bare Green's functions is exact only in the lowest order in the tunnel Hamiltonian. Since the results of the nonlocal transport depend on the nature of electron propagation in the electrodes, we consider below the limits of clean and dirty superconductors.

A. Clean superconductor

In a clean superconductor, the electron mean free path is much longer than the BCS coherence length ($l_e \gg \xi_0 = \hbar v_F/\pi\Delta$), and the motion is described as being ballistic. The first three terms in (14) are nonzero for voltages above the superconducting gap. They can be calculated by using the expressions for the bare Green's functions provided in Appendices A and B. These three terms stand for the electron transfer between the electrodes with the quasiparticle creation in the superconductor, electron transfer with creation or annihilation of pairs in the intermediate state, and the branch crossing processes in the Blonder-Tinkham-Klapwijk formalism [28], respectively. For the single junction case between two normal metal electrodes ($t^{(b)}, \Delta \to 0$), and for vanishing circuit impedance ($z = \mathrm{Re}[Z_T(\omega = 0)]/R_K \to 0$; $R_K = h/e^2$), the first term gives the Landauer result, $I^{(a)}_{NN} = \frac{2e^2}{h} T^{(a)}_{\mathrm{eff}} V_a$, where $T^{(a)}_{\mathrm{eff}} = \frac{4\pi\Gamma^{(a)}}{(1+\pi\Gamma^{(a)})^2}$ is the effective transmission coefficient; $\Gamma^{(a)} = \pi \nu_a \nu_c |t^{(a)}|^2$, and ν_a and ν_c are the densities of states per spin and per unit volume at the Fermi level in the electrodes a and c, respectively.

The last term in (14) is nonzero for voltages below, as well as above the superconducting gap, and is of main interest with regard to operation of the device as a generator of mobile pairs of spin-entangled electrons. For $\mu = a$ and $i = 2$, this term represents the direct Andreev reflection current. In the single junction case [29], for vanishing circuit impedance and at zero temperature, we have for $eV_a \leqslant \Delta$:

$$I^{(a)}_{DA} = \frac{4\pi\Gamma^{(a)2}}{1-(\pi\Gamma^{(a)})^4} \ln\left(\frac{1+v}{1-v}\right)\frac{e\Delta}{\hbar},$$
$$v = \frac{1-(\pi\Gamma^{(a)})^2}{1+(\pi\Gamma^{(a)})^2}\frac{eV_a}{\Delta}. \qquad (15)$$

In contrast to the calculations involving perturbative expansions to finite order in the tunnel Hamiltonian and producing diverging results for voltages at the superconducting energy gap [15,30], originating from the singularity of the bare local BCS Green's functions, the present approach provides nondiverging results.

The other contributions of the last term in (14) result from processes involving both normal metal electrodes: elastic cotunneling for $\mu = b$ and $i = 1$, and crossed Andreev reflection for $\mu = b$ and $i = 2$. They are represented diagrammatically in Fig. 3. In the lowest order in the tunnel matrix elements [15,31,32], that is, by substituting the bare Green's functions $g^R_{cc1i}(\mathbf{x}_a, \mathbf{x}_\mu; \epsilon)$ for the dressed Green's functions $G^R_{cc1i}(\mathbf{x}_a, \mathbf{x}_\mu; \epsilon)$ $(i = 1,2)$, in the superconducting electrode and after summation over spin, we get in the zero temperature limit

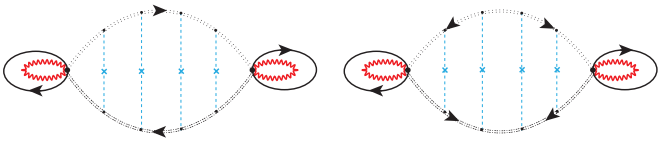

FIG. 3. Diagrammatic representation of the coordinate-energy space contribution of the last term in (14) for $\mu = b$. The diagram on the left depicts elastic cotunneling ($i = 1$), while the one on the right depicts crossed Andreev reflection ($i = 2$). The solid lines stand for the bare lesser and greater Green's functions for electrons in the normal metal electrodes, wiggly lines represent phase correlators, and dotted (dash-dotted) lines represent full retarded (advanced) Green's functions in the superconducting electrode. These are normal and anomalous Green's functions in the case of elastic cotunneling and crossed Andreev reflection, respectively. In the case of the diffusive superconducting electrode (Sec. II B), we consider impurity scattering (indicated on the diagrams by dashed lines with crosses). The probability of quantum diffusion is obtained by iterating to infinity a series of these scattering processes.

and for low voltages ($eV_\alpha \ll \Delta$):

$$I^{(a)}_{\substack{EC\\CAR}} = 4\frac{e\pi}{\hbar}\Gamma^{(a)}\Gamma^{(b)}\mathfrak{r}^2\begin{bmatrix}\cos^2(k_F\delta r)\\ \sin^2(k_F\delta r)\end{bmatrix} \times \frac{e^{-4\gamma z}}{\Gamma(2+4z)}\,\mathrm{sgn}(eV_a \mp eV_b)\frac{|eV_a \mp eV_b|^{1+4z}}{(\hbar\omega_R)^{4z}}, \qquad (16)$$

where $\mathfrak{r} = e^{-\delta r/\pi\xi_0}/(k_F\delta r)$, with δr being the distance between the junctions, and k_F the Fermi wave vector; γ denotes the Euler constant and $\omega_R = 1/(RC)$ is the inverse classical charge relaxation time. In deriving (16), we assumed that both junctions have the same capacitance, $C_1 = C_2 = C$, and that impedances in both normal metal branches are purely ohmic, $Z_1 = Z_2 = R$. Figure 4 shows the numerical results obtained from Eq. (14) for the elastic cotunneling current, crossed Andreev reflection current, and the low voltage analytic result for these currents, Eq. (16), averaged over Fermi oscillations.

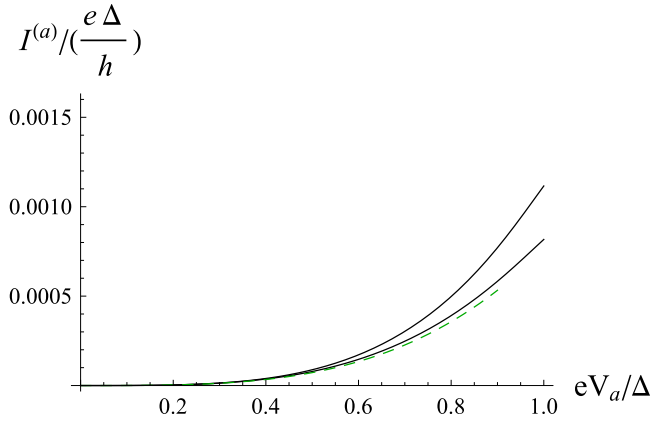

FIG. 4. The numerical results from formula (14) for the elastic cotunneling current, $I^{(a)}_{EC}$ (top curve) and the crossed Andreev current, $I^{(a)}_{CAR}$ (middle curve) as functions of the voltage across the junction a; the analytic result for these currents given by the formula (16), valid in the low voltage limit, is shown as a dashed curve. Parameter values are $eV_b = 0$, $k_F\delta r = 10$, $z = 0.6$, $\Gamma^{(a)} = \Gamma^{(b)} = 0.1$, $\Delta/E_c = 1.25$, $\Delta/E_F = 2 \times 10^{-5}$.

By differentiating the total current through the junction a with respect to voltage V_b, we obtain the expression for the nonlocal differential conductance in the tunneling limit,

$$\mathcal{G}_{ab} \equiv \frac{\partial I^{(a)}}{\partial V_b} = 4\pi^2(1+4z)\Gamma^{(a)}\Gamma^{(b)}\mathfrak{r}^2\frac{e^{-4\gamma z}}{\Gamma(2+4z)} \times\left[\left(\frac{|eV_a+eV_b|}{\hbar\omega_R}\right)^{4z}-\left(\frac{|eV_a-eV_b|}{\hbar\omega_R}\right)^{4z}\right]\frac{e^2}{h}. \quad (17)$$

The analytic result can also be obtained when taking into account tunnel Hamiltonian contributions to infinite order but for vanishing circuit impedance. In the region of low voltages ($eV_\alpha \ll \Delta$) and for zero temperature it is given by

$$I^{(a)}_{\substack{EC\\CAR}} = \frac{4e^2}{\hbar}\pi\Gamma^{(a)}\Gamma^{(b)}\mathfrak{r}^2\mathcal{F}_{\substack{EC\\CAR}}(k_F\delta r)(V_a \mp V_b),$$

$$\mathcal{F}_i(k_F\delta r) = \frac{a_i\cos^2(k_F\delta r)+b_i\sin^2(k_F\delta r)}{[c\cos(2k_F\delta r)+1]^2 d^2} \quad (i = EC, CAR),$$

$$\begin{bmatrix}a_{EC}\\ b_{CAR}\end{bmatrix} = [1+(\mathfrak{r}^2\pm 1)\pi^2\Gamma^{(a)}\Gamma^{(b)}]^2,$$

$$\begin{bmatrix}b_{EC}\\ a_{CAR}\end{bmatrix} = \pi^2(\Gamma^{(a)}\pm\Gamma^{(b)})^2, \quad c = \frac{2\mathfrak{r}^2\pi^4\Gamma^{(a)2}\Gamma^{(b)2}}{d},$$

$$d = 1+2\pi^2\mathfrak{r}^2\Gamma^{(a)}\Gamma^{(b)}+\pi^2(\Gamma^{(a)2}+\Gamma^{(b)2}) +\pi^4(1+\mathfrak{r}^4)\Gamma^{(a)2}\Gamma^{(b)2}. \quad (18)$$

From the above expression, we obtain the nonlocal differential conductance,

$$\mathcal{G}_{ab} = \frac{4e^2}{\hbar}\pi\Gamma^{(a)}\Gamma^{(b)}\mathfrak{r}^2(\bar{\mathcal{F}}_{CAR}-\bar{\mathcal{F}}_{EC}), \quad (19)$$

where on the right-hand side we introduce the averages over the Fermi oscillations $\bar{\mathcal{F}}_i = \frac{1}{2\pi}\int_0^{2\pi} d\phi\,\mathcal{F}_i(\phi) = \frac{1}{2d^2\sqrt{1-c^2}}(\frac{a_i}{1+c}+\frac{b_i}{1-c})$, where $\phi = k_F\delta r$. In the lowest order of the series expansion in $\mathfrak{r}^2$, we have

$$\mathcal{G}_{ab} = -32\frac{e^2\mathfrak{r}^2}{h}\frac{(\pi^2\Gamma^{(a)}\Gamma^{(b)})^2}{[1+\pi^2(\Gamma^{(a)2}+\Gamma^{(b)2})+\pi^4\Gamma^{(a)2}\Gamma^{(b)2}]^2}. \quad (20)$$

For low transparency barriers, $T^{(a)}_{\rm eff}, T^{(b)}_{\rm eff} \ll 1$, the nonlocal differential conductance behaves as $\mathcal{G}_{ab} \propto T^{(a)2}_{\rm eff}T^{(b)2}_{\rm eff}$; for highly asymmetric barriers, e.g., $T^{(a)}_{\rm eff}\sim 1$, $T^{(b)}_{\rm eff}\ll 1$, it scales as $\mathcal{G}_{ab}\propto T^{(b)2}_{\rm eff}$.

B. Dirty superconductor

When disorder is present in the superconducting electrode, it gives rise to a random impurity potential which scatters electrons. A superconductor is said to be in the dirty limit [30,33–37] when the concentration of defects is high enough that the elastic mean free path becomes much shorter than the BCS coherence length ($l_e \ll \xi_0$). We will assume the presence of nonmagnetic impurities that give rise to a white noise potential, and will consider the weak disorder limit, $k_F l_e \gg 1$. In this regime, after each collision one may asymptotically reconstruct a free wave, and obtain the self-energy of the Schrödinger equation by summing over a series of scattering events assuming that they are independent. The superconductor bare Green's functions become dressed by impurity scattering and are short ranged, e.g., $\langle\langle g^{R,A}_{cc11}(\mathbf{x},\mathbf{x}';\epsilon)\rangle\rangle = g^{R,A}_{cc11}(\mathbf{x},\mathbf{x}';\epsilon)e^{-|\mathbf{r}-\mathbf{r}'|/2l_e}$, where $\langle\langle\cdots\rangle\rangle$ indicates impurity averaging. The relevant long-range physical properties of the system in this case are therefore not determined by the average Green's functions, but by the impurity averaged products of (retarded and advanced) Green's functions. To obtain these averaged products, we expand the $\mathbf{r}$-representation Green's functions into a complete set of functions, $\chi_{\mathbf{k}}(\mathbf{r})$, satisfying the Schrödinger equation with the random potential; for example, $g^R_{cc11}(\mathbf{r}\sigma,\mathbf{r}'\sigma';\epsilon) = \sum_{\mathbf{k},\mathbf{k}'}\chi_{\mathbf{k}}(\mathbf{r})g^R_{cc11}(\mathbf{k}\sigma,\mathbf{k}'\sigma';\epsilon)\chi^*_{\mathbf{k}'}(\mathbf{r}')$. The impurity averaged products (listed in Appendix C) are then obtained with the aid of the spectral function $K_\epsilon(\mathbf{r},\mathbf{r}') = \sum_{\mathbf{k}}\chi_{\mathbf{k}}(\mathbf{r})\chi^*_{\mathbf{k}}(\mathbf{r}')\delta(\epsilon-\epsilon_{\mathbf{k}})$, related to the diffuson $\mathcal{P}(\mathbf{r},\mathbf{r}',\epsilon_0)$ as $\langle\langle K_\epsilon(\mathbf{r},\mathbf{r}')K_{\epsilon+\epsilon_0}(\mathbf{r},\mathbf{r}')\rangle\rangle = [\mathcal{P}(\mathbf{r},\mathbf{r}',\epsilon_0)+\mathcal{P}(\mathbf{r},\mathbf{r}',-\epsilon_0)]\nu_c/2\pi$; $\mathcal{P}(\mathbf{r},\mathbf{r}',\epsilon_0)$ is the Fourier transform of the average probability $\mathcal{P}(\mathbf{r},\mathbf{r}',t)$ that a particle leaving a point $\mathbf{r}$ will propagate to $\mathbf{r}'$ during the time interval t.

In the tunneling limit, by substituting the expressions from Appendix C into the Eq. (14), for ballistic transport [in which case, $\mathcal{P}(\mathbf{r}_a,\mathbf{r}_b,t) = \delta(\delta r - v_F t)/4\pi\delta r^2$] we recover the result (16) averaged over Fermi wavelength scale. For diffusive transport, in Eq. (16), $\mathfrak{r}^2\cos^2(k_F\delta r)$ for EC and $\mathfrak{r}^2\sin^2(k_F\delta r)$ for CAR are replaced by $\bar{\mathcal{P}}(\delta r,\frac{2\Delta}{\hbar})/\pi\hbar\nu_c$. Here, $\bar{\mathcal{P}}(\mathbf{r},\mathbf{r}',s)$ denotes the Laplace transform of $\mathcal{P}(\mathbf{r},\mathbf{r}',t)$ satisfying the equation

$$(s-D\Delta)\bar{\mathcal{P}}(\mathbf{r},\mathbf{r}',s) = \delta(\mathbf{r}-\mathbf{r}'), \quad (21)$$

where $D = v_F l_e/d$ is the diffusion constant in d dimensions. The function $\bar{\mathcal{P}}$ provides the time integrated probability for a particle of lifetime $\tau_s = 1/s$, leaving $\mathbf{r}$ to arrive at $\mathbf{r}'$. Solution of the above equation (21) depends on the boundary conditions provided by the shape of the superconducting electrode. In the absence of disorder, free propagation for $d = 3$ is described by $\bar{\mathcal{P}}^{(3)}(\delta r,s) = e^{-\delta r/v_F\tau_s}/4\pi\delta r^2 v_F$. With disorder present, we have $\bar{\mathcal{P}}^{(3)}(\delta r,s) = e^{-\delta r/l_s}/4\pi D\delta r$, where $l_s = \sqrt{D\tau_s}$ stands for the diffusion length.

For vanishing circuit impedance ($z = 0$), by following the procedure indicated in Appendix D, one can arrive at the expression for the nonlocal differential conductance to all orders in the tunnel Hamiltonian,

$$\mathcal{G}_{ab} = -64\frac{e^2}{h}\frac{\Delta^2-(eV_b)^2}{\Delta^2}\frac{\bar{\mathcal{P}}\left[\mathbf{r}_a,\mathbf{r}_b,\frac{2}{\hbar}\sqrt{\Delta^2-(eV_b)^2}\right]}{\pi\hbar\nu_c} \times\prod_{\alpha=a,b}\frac{(\pi\Gamma^{(\alpha)}\Delta)^2}{[1+(\pi\Gamma^{(\alpha)})^2]^2\Delta^2-[1-(\pi\Gamma^{(\alpha)})^2]^2(eV_b)^2}. \quad (22)$$

Without disorder, the above formula gives the result for the case of ballistic motion considered in Sec. II A, averaged over the directions of the Fermi wave vector. If the distance between the junctions is small compared to the coherence length $\delta r \ll \xi_d = \sqrt{\hbar D/\Delta}$, so that the exponential terms in $\bar{\mathcal{P}}^{(3)}(\delta r,s)$ can be neglected, the ratio between the nonlocal differential conductances in the diffusive and ballistic cases is equal to $3\delta r/l_e$. Therefore, for junction distances of the order and greater than the elastic mean free path the nonlocal differential

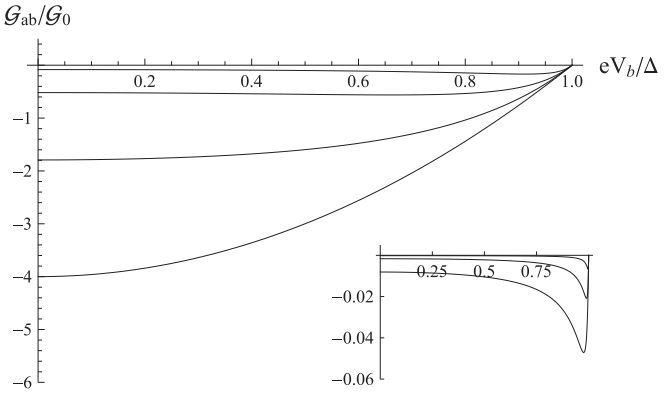

FIG. 5. Nonlocal differential conductance $\mathcal{G}_{ab}$, in units $\mathcal{G}_0$, as a function of voltage eV_b, for $\delta r \ll \xi_d$. In three dimensions $\mathcal{G}_0 = e^2/2h(k_F\delta r)^2$ in the ballistic case and $\mathcal{G}_0 = 3e^2/2hk_F^2\delta r l_e$ in the diffusive case. By decreasing the barrier transmission the curves get closer to the horizontal axis, $T_{\rm eff}^{(a)} = T_{\rm eff}^{(b)} = 1,0.9,0.75,0.55$ (main plot), and 0.35,0.25,0.15 (inset).

conductance in the diffusive limit dominates over the ballistic limit. Figure 5 shows $\mathcal{G}_{ab}$ as a function of the voltage V_b for a set of values of the tunnel junction transparencies.

In lower dimensions, the boundaries of a thin film of a thickness t, or a narrow wire of a diameter t, provide the limits on the elastic mean free path. For $t \ll \xi_0$ the corresponding electron propagation becomes quasi-two-dimensional and quasi-one-dimensional diffusion in the case of a film and a wire, respectively. The corresponding probability in two dimensions is $\bar{\mathcal{P}}^{(2)}(\delta r,s) = K_0(\delta r/l_s)/2\pi D$, where K_0 is the modified Bessel function of the second kind. In one dimension we have $\bar{\mathcal{P}}^{(1)}(\delta r,s) = l_s e^{-\delta r/l_s}/2D$. The associated densities of states in (22) are given by $\nu_c^{(2)} = m_e/2\pi\hbar^2$ and $\nu_c^{(1)} = m_e/\pi k_F\hbar^2$.

For nonvanishing circuit impedance, by using Eqs. (D1) and (D2) from Appendix D, one can obtain the variation of the nonlocal differential conductance as a function of junction transparencies, as shown in Fig. 6. In Ref. [24], the effects of electron-electron interactions were treated perturbatively ($z \ll 1$), by expansion to the lowest order of the relevant term in the action within the path integral formalism. We show a comparison of the result of that study, given by the formulas (46) and (47) in Ref. [24] (blue line in the top diagram in Fig. 6), to our result (red line in the top diagram in Fig. 6). While in the case of vanishing circuit impedance ($z = 0$), the nonlocal conductance is always nonpositive, with increasing circuit impedance the sign of the nonlocal conductance depends on the voltages applied to the normal metal electrodes and the transparencies of the barriers. For sufficiently high circuit impedance, the dynamic Coulomb blockade makes the crossed Andreev reflection contribution dominant over the elastic cotunneling and the nonlocal conductance becomes non-negative.

III. CONCLUSIONS

In this paper, we developed the theory of nonlocal electron transport, based on Nambu-Gor'kov and Schwinger-Keldysh formalisms, for the three-terminal Cooper-pair splitting device. The theory accounts for the effects of the general electromagnetic environment and the arbitrary interface transmissions between the superconducting and the normal metal leads. We considered the interplay between the elastic

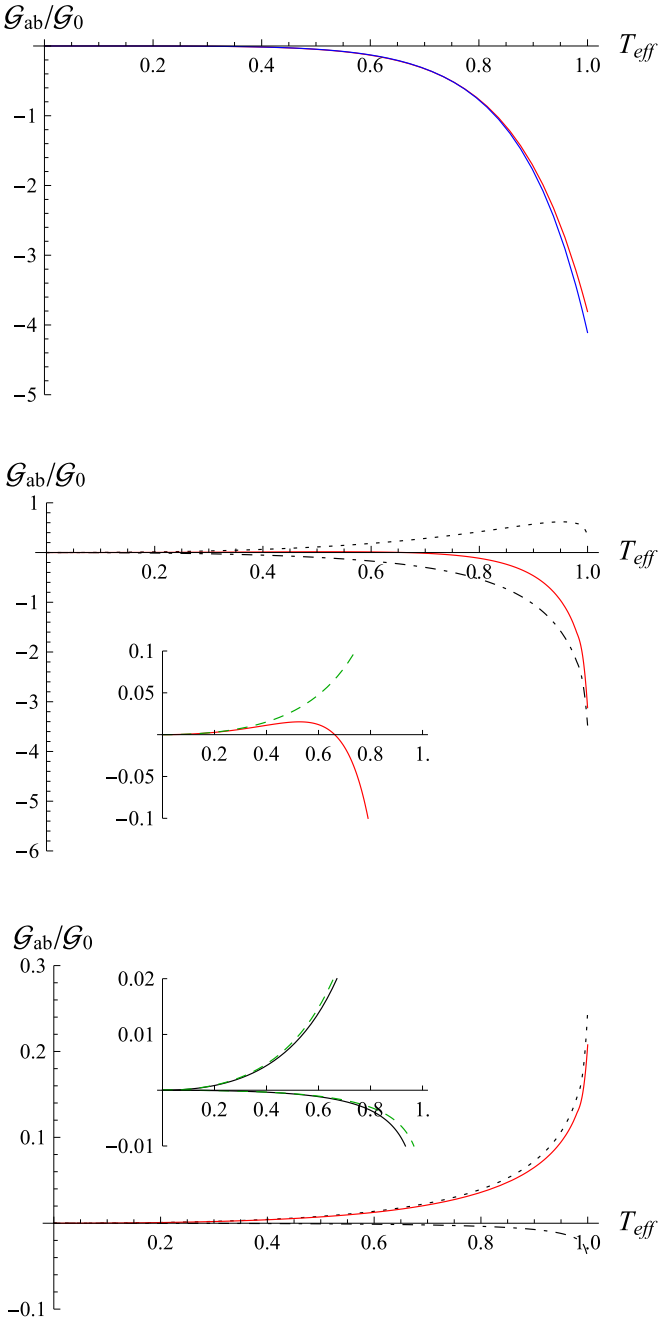

FIG. 6. Nonlocal differential conductance $\mathcal{G}_{ab}$, in units $\mathcal{G}_0 = 2e^2\bar{\mathcal{P}}(\delta r,2\Delta/\hbar)/h^2\nu_c$, as a function of the effective transmission coefficient $T_{\rm eff}^{(a)} = T_{\rm eff}^{(b)} = T_{\rm eff}$, for $z = 0.001$ (top plot), $z = 0.06$ (middle plot), and $z = 0.6$ (bottom plot); $eV_a = 0.2\Delta$, $eV_b = 0.1\Delta$. In the top plot, the blue line is the result from Ref. [24]. Dotted lines represent contributions from the crossed-Andreev reflection, dash-dotted lines those of the elastic cotunneling, and solid (red) lines the total nonlocal differential conductance. The inset in the middle plot shows a zoom-in in the region where $\mathcal{G}_{ab}$ changes sign, and the inset in the bottom plot shows the crossed-Andreev reflection and elastic cotunneling contributions; in both insets the dashed lines show the corresponding analytic results valid in the limit of low interface transmissions.

cotunneling and the crossed-Andreev reflection processes, and showed the influence of the circuit impedance on the nonlocal differential conductance, $\mathcal{G}_{ab}$. In the tunneling limit, Eq. (17), we obtain nonzero nonlocal differential conductance for finite circuit impedance and nonzero voltages applied to the normal metal leads. It was shown in Ref. [20] that nonzero nonlocal differential conductance can result from the electromagnetic modes coupling the charge fluctuations on different junctions. Here, we show that even without this coupling the dissipative impedance causes nonzero $\mathcal{G}_{ab}$. With increasing junction transmittances, for low circuit impedance the EC contribution dominates and $\mathcal{G}_{ab} < 0$; for higher values of the circuit impedance the dynamic Coulomb blockade makes the CAR contribution dominant and as a consequence $\mathcal{G}_{ab} > 0$.

In the weak disorder limit considered here, the self-energy corresponding to the single electron Schrödinger equation is represented by irreducible diagrams corresponding to independent collisions. Using the Matthiessen rule, contributions of other scattering processes can be included by defining the imaginary part of the self-energy via the total scattering time that includes in addition to scattering from static impurities also other mechanisms. In this way, spin-orbit and charge imbalance can be included in our formalism [38].

We performed expansion in the lowest order of diffuson in solving Eq. (D3). Higher order terms resulting from averages of diagonal Green's functions (of the form $\langle\langle g^R_{ccij}(\mathbf{x}_a,\mathbf{x}_a;\epsilon) g^A_{ccij}(\mathbf{x}_b,\mathbf{x}_b;\epsilon-\omega)\rangle\rangle$) can be expressed in terms of the squares of diffusons. Including higher order correlation functions due to electromagnetic environment modes would also increase the accuracy of our approximation for voltages approaching the superconducting gap.

We neglected the inverse proximity effect in the superconductor near the interfaces with the normal metal electrodes. Such assumption is justified as long as the linear dimension of the contacts is small compared to the superconducting coherence length. It would be of interest to consider extended contacts and incorporate the results of the strong nonequilibrium effects on the superconducting order parameter, as obtained in the self-consistent model calculations [18].

Finally, we point out that our approach is applicable to a variety of materials used for the Cooper-pair splitter, such as those listed in the Introduction. For each particular setup, one needs to use the appropriate Green's functions. For example, for the Tomonaga-Luttinger liquid electrodes connected to a superconductor, the Green's functions were considered in [39].

APPENDIX A: COORDINATE REPRESENTATION OF THE BARE GREEN'S FUNCTIONS IN THE NORMAL METAL ELECTRODES

The greater and lesser Green's functions in the normal metal electrodes are given by

$$
\begin{aligned}
&g^{>}_{\tilde{\alpha}\tilde{\alpha}11}(\mathbf{x}_\alpha,\mathbf{x}_\alpha;\omega)\\
&\quad= -2i\pi\hbar\nu_\alpha\int_{-\infty}^{\infty} d\epsilon_{\mathbf{k}} P_\alpha(\hbar\omega+eV_\alpha-\epsilon_{\mathbf{k}})[1-f(\epsilon_{\mathbf{k}})],\\
&g^{<}_{\tilde{\alpha}\tilde{\alpha}11}(\mathbf{x}_\alpha,\mathbf{x}_\alpha;\omega)\\
&\quad= 2i\pi\hbar\nu_\alpha\int_{-\infty}^{\infty} d\epsilon_{\mathbf{k}} P_\alpha(\epsilon_{\mathbf{k}}-eV_\alpha-\hbar\omega) f(\epsilon_{\mathbf{k}}),\\
&g^{>}_{\tilde{\alpha}\tilde{\alpha}22}(\mathbf{x}_\alpha,\mathbf{x}_\alpha;\omega)\\
&\quad= -2i\pi\hbar\nu_\alpha\int_{-\infty}^{\infty} d\epsilon_{\mathbf{k}} P_\alpha(\hbar\omega+\epsilon_{\mathbf{k}}-eV_\alpha) f(\epsilon_{\mathbf{k}}),\\
&g^{<}_{\tilde{\alpha}\tilde{\alpha}22}(\mathbf{x}_\alpha,\mathbf{x}_\alpha;\omega)\\
&\quad= 2i\pi\hbar\nu_\alpha\int_{-\infty}^{\infty} d\epsilon_{\mathbf{k}} P_\alpha(eV_\alpha-\epsilon_{\mathbf{k}}-\hbar\omega)[1-f(\epsilon_{\mathbf{k}})], \quad \text{(A1)}
\end{aligned}
$$

where the probability of the tunneling electron exchanging the energy ϵ with the environment [27] is given by $P_\alpha(\epsilon)=\frac{1}{2\pi\hbar}\int_{-\infty}^{\infty} dt\, e^{J_\alpha(t)+i\epsilon t/\hbar}$, with the phase correlation function given by $J_\alpha(t)=\langle[\tilde{\phi}_\alpha(t)-\tilde{\phi}_\alpha(0)]\tilde{\phi}_\alpha(0)\rangle = 2\int_0^\infty \frac{d\omega}{\omega}\frac{\mathrm{Re}Z_\alpha(\omega)}{R_K}\{\coth(\frac{1}{2}\beta\hbar\omega)[\cos(\omega t)-1]-i\sin(\omega t)\}$. The retarded and advanced Green's functions are given by

$$
\begin{aligned}
g^R_{\tilde{\alpha}\tilde{\alpha}11}(\mathbf{x}_\alpha,\mathbf{x}_\alpha;\omega) &= g^{A*}_{\tilde{\alpha}\tilde{\alpha}11}(\mathbf{x}_\alpha,\mathbf{x}_\alpha;\omega) = -i\pi\hbar\nu_\alpha\left\{1+\int_{-\infty}^{\infty}\frac{d\omega'}{2\pi} i\mathfrak{F}^{(\alpha)R}_{+-}(\omega')\tanh\left[\frac{\hbar\omega-\hbar\omega'+eV_\alpha}{2k_BT}\right]\right\},\\
g^R_{\tilde{\alpha}\tilde{\alpha}22}(\mathbf{x}_\alpha,\mathbf{x}_\alpha;\omega) &= g^{A*}_{\tilde{\alpha}\tilde{\alpha}22}(\mathbf{x}_\alpha,\mathbf{x}_\alpha;\omega) = -i\pi\hbar\nu_\alpha\left\{1+\int_{-\infty}^{\infty}\frac{d\omega'}{2\pi} i\mathfrak{F}^{(\alpha)R}_{-+}(\omega')\tanh\left[\frac{\hbar\omega-\hbar\omega'-eV_\alpha}{2k_BT}\right]\right\}, \quad \text{(A2)}
\end{aligned}
$$

where $\mathfrak{F}^{(\alpha)}_{\eta\bar{\eta}}(\omega')$ is the Fourier transform of $\mathfrak{F}^{(\alpha)}_{\eta\bar{\eta}}(t,t') = -i\langle \mathcal{T}_c e^{i\eta\tilde{\phi}_\alpha(t)} e^{i\bar{\eta}\tilde{\phi}_\alpha(t')}\rangle$, $(\eta,\bar{\eta})=(\pm,\mp)$. The off-diagonal Green's functions in the normal metal electrodes vanish, e.g., $g^R_{\tilde{\alpha}\tilde{\alpha}12}(\mathbf{x}_\alpha,\mathbf{x}_\alpha;\omega) = g^R_{\tilde{\alpha}\tilde{\alpha}21}(\mathbf{x}_\alpha,\mathbf{x}_\alpha;\omega) = 0$.

APPENDIX B: BARE GREEN'S FUNCTIONS IN THE SUPERCONDUCTING ELECTRODE (CLEAN LIMIT)

The nonlocal lesser Green's functions are given by

$$
\begin{aligned}
\begin{bmatrix} g^<_{cc11}(\mathbf{x}_\alpha,\mathbf{x}_\beta;\omega)\\ g^<_{cc22}(\mathbf{x}_\alpha,\mathbf{x}_\beta;\omega)\end{bmatrix} &= 2i\pi\hbar\nu_c\frac{|\hbar\omega|}{\sqrt{(\hbar\omega)^2-\Delta^2}} f(\hbar\omega)\Theta(|\hbar\omega|-\Delta)\delta_{\sigma,\sigma'}\left[\frac{\sin(k_F\delta r)}{k_F\delta r}\cos\left(\sqrt{(\hbar\omega)^2-\Delta^2}\frac{\delta r}{\pi\xi_0\Delta}\right)\right.\\
&\left.\pm\frac{\cos(k_F\delta r)}{k_F\delta r}\sin\left(\sqrt{(\hbar\omega)^2-\Delta^2}\frac{\delta r}{\pi\xi_0\Delta}\right)\frac{\sqrt{(\hbar\omega)^2-\Delta^2}}{\hbar\omega}\right],
\end{aligned}
$$

$$g^{<}_{cc12}(\mathbf{x}_\alpha,\mathbf{x}_\beta;\omega) = g^{<}_{cc21}(\mathbf{x}_\alpha,\mathbf{x}_\beta;\omega)$$
$$= -2i\pi\hbar\nu_c\,\mathrm{sgn}(\sigma)\,\mathrm{sgn}(\omega)\frac{\Delta}{\sqrt{(\hbar\omega)^2-\Delta^2}}f(\hbar\omega)\Theta(|\hbar\omega|-\Delta)\delta_{\sigma,\sigma'}\frac{\sin(k_F\delta r)}{k_F\delta r}\cos\left(\sqrt{(\hbar\omega)^2-\Delta^2}\frac{\delta r}{\pi\xi_0\Delta}\right). \quad \text{(B1)}$$

The expressions for the greater Green's functions are obtained from the corresponding expressions above by substituting $-f(-\hbar\omega)$ in place of $f(\hbar\omega)$. The retarded and advanced Green's functions are given by

$$\begin{bmatrix} g^R_{cc11}(\mathbf{x}_\alpha,\mathbf{x}_\beta;\omega) \\ g^R_{cc22}(\mathbf{x}_\alpha,\mathbf{x}_\beta;\omega)\end{bmatrix} = \begin{bmatrix} g^{A*}_{cc11}(\mathbf{x}_\alpha,\mathbf{x}_\beta;\omega) \\ g^{A*}_{cc22}(\mathbf{x}_\alpha,\mathbf{x}_\beta;\omega)\end{bmatrix} = -\delta_{\sigma,\sigma'}\pi\hbar\nu_c\frac{\exp\left[-\frac{\delta r}{\pi\xi_0\Delta}\sqrt{\Delta^2-(\hbar\omega)^2}\right]}{k_F\delta r}$$
$$\times\left[\sin(k_F\delta r)\frac{\hbar\omega}{\sqrt{\Delta^2-(\hbar\omega)^2}}\pm\cos(k_F\delta r)\right] \quad (\Delta > |\hbar\omega|),$$

$$\begin{bmatrix} g^R_{cc11}(\mathbf{x}_\alpha,\mathbf{x}_\beta;\omega) \\ g^R_{cc22}(\mathbf{x}_\alpha,\mathbf{x}_\beta;\omega)\end{bmatrix} = \begin{bmatrix} g^{A*}_{cc11}(\mathbf{x}_\alpha,\mathbf{x}_\beta;\omega) \\ g^{A*}_{cc22}(\mathbf{x}_\alpha,\mathbf{x}_\beta;\omega)\end{bmatrix} = -\delta_{\sigma,\sigma'}\pi\hbar\nu_c\frac{\exp\left[i\frac{\delta r}{\pi\xi_0\Delta}\sqrt{(\hbar\omega)^2-\Delta^2}\,\mathrm{sgn}(\omega)\right]}{k_F\delta r}$$
$$\times\left[i\sin(k_F\delta r)\frac{|\hbar\omega|}{\sqrt{(\hbar\omega)^2-\Delta^2}}\pm\cos(k_F\delta r)\right] \quad (\Delta < |\hbar\omega|),$$

$$g^R_{cc12}(\mathbf{x}_\alpha,\mathbf{x}_\beta;\omega) = g^R_{cc21}(\mathbf{x}_\alpha,\mathbf{x}_\beta;\omega) = g^{A*}_{cc12}(\mathbf{x}_\alpha,\mathbf{x}_\beta;\omega) = g^{A*}_{cc21}(\mathbf{x}_\alpha,\mathbf{x}_\beta;\omega)$$
$$= \begin{cases} \delta_{\sigma,\sigma'}\,\mathrm{sgn}(\sigma)\pi\hbar\nu_c e^{-(\delta r/\pi\xi_0\Delta)\sqrt{\Delta^2-(\hbar\omega)^2}}\frac{\sin(k_F\delta r)}{k_F\delta r}\frac{\Delta}{\sqrt{\Delta^2-(\hbar\omega)^2}} & (\Delta > |\hbar\omega|), \\ i\delta_{\sigma,\sigma'}\,\mathrm{sgn}(\sigma)\,\mathrm{sgn}(\omega)\pi\hbar\nu_c e^{i(\delta r/\pi\xi_0\Delta)\,\mathrm{sgn}(\omega)\sqrt{(\hbar\omega)^2-\Delta^2}}\frac{\sin(k_F\delta r)}{k_F\delta r}\frac{\Delta}{\sqrt{(\hbar\omega)^2-\Delta^2}} & (\Delta < |\hbar\omega|). \end{cases} \quad \text{(B2)}$$

The expressions for the local Green's functions, corresponding to $\mathbf{r}_\alpha = \mathbf{r}_\beta$, are obtained from the corresponding functions above by taking the limit $\delta r \to 0$ in the terms proportional to $\sin(k_F\delta r)$, and neglecting the terms proportional to $\cos(k_F\delta r)$.

APPENDIX C: IMPURITY AVERAGED PRODUCTS OF BARE GREEN'S FUNCTIONS IN THE SUPERCONDUCTING ELECTRODE (DIRTY LIMIT)

The impurity averaged products of Green's functions are given by

$$\langle\langle|g^R_{ccij}(\mathbf{x}_\alpha,\mathbf{x}_\beta;\omega)|^2\rangle\rangle = \hbar\pi\,\nu_c\delta_{\sigma,\sigma'}\frac{\Delta^2}{\Delta^2-(\hbar\omega)^2}\bar{\mathcal{P}}\left(\delta r,\frac{2}{\hbar}\sqrt{\Delta^2-(\hbar\omega)^2}\right) \quad (i,j=1,2),$$
$$\langle\langle g^R_{ccii}(\mathbf{x}_\alpha,\mathbf{x}_\beta;\omega)g^A_{ccij}(\mathbf{x}_\beta,\mathbf{x}_\alpha;\omega)\rangle\rangle = -\hbar\pi\,\nu_c\delta_{\sigma,\sigma'}\frac{\hbar\omega\Delta\sigma}{\Delta^2-(\hbar\omega)^2}\bar{\mathcal{P}}\left(\delta r,\frac{2}{\hbar}\sqrt{\Delta^2-(\hbar\omega)^2}\right) \quad (i\neq j),$$
$$\langle\langle g^R_{ccii}(\mathbf{x}_\alpha,\mathbf{x}_\beta;\omega)g^A_{ccjj}(\mathbf{x}_\beta,\mathbf{x}_\alpha;\omega)\rangle\rangle = -\hbar\pi\,\nu_c\delta_{\sigma,\sigma'}\frac{\Delta^2-2(\hbar\omega)^2}{\Delta^2-(\hbar\omega)^2}\bar{\mathcal{P}}\left(\delta r,\frac{2}{\hbar}\sqrt{\Delta^2-(\hbar\omega)^2}\right) \quad (i\neq j). \quad \text{(C1)}$$

In the weak disorder regime, $k_F l_e \gg 1$, one can show that the average probability $\mathcal{P}(\mathbf{r}_1,\mathbf{r}_2,\epsilon)$ can be expressed via the integral

$$\mathcal{P}(\mathbf{r}_1,\mathbf{r}_2,\epsilon) = 2\pi\,\nu_c\int d\mathbf{r}\,d\mathbf{r}'\mathcal{P}_0(\mathbf{r}_1,\mathbf{r},\epsilon)\Phi(\mathbf{r},\mathbf{r}',\epsilon)\mathcal{P}_0(\mathbf{r}',\mathbf{r}_2,\epsilon), \quad \text{(C2)}$$

where $\mathcal{P}_0(\mathbf{r}_1,\mathbf{r}_2,\epsilon)$ is the probability for a particle of energy ϵ to propagate between the points $\mathbf{r}_1$ and $\mathbf{r}_2$ without any collision. The structure factor satisfies the Bethe-Salpeter equation:

$$\Phi(\mathbf{r},\mathbf{r}',\epsilon) = \frac{\delta(\mathbf{r}-\mathbf{r}')}{2\pi\,\nu_c\tau_e} + \frac{1}{\tau_e}\int d\mathbf{r}''\Phi(\mathbf{r},\mathbf{r}'',\epsilon)\mathcal{P}_0(\mathbf{r}'',\mathbf{r}',\epsilon). \quad \text{(C3)}$$

Variations of $\Phi(\mathbf{r},\mathbf{r}',\epsilon)$ are small on the scale of l_e allowing the expansion around $\mathbf{r}''$, which simplifies the above integrals. In this way one can show that the probability $\mathcal{P}(\mathbf{r}_1,\mathbf{r}_2,\epsilon)$ satisfies a diffusion equation.

APPENDIX D: NONLOCAL DIFFERENTIAL CONDUCTANCE

Taking a derivative of the expression for the current (14), we get for $|V_a| > |V_b|$ in the zero temperature limit:

$$\mathcal{G}^{CAR}_{ab} = 8\pi^2\Gamma^{(a)}\Gamma^{(b)}\frac{e^2}{h}\frac{1}{(\pi\hbar\nu_c)^2}\int_{-eV_a}^{eV_b}d\xi\int_0^{eV_a+\xi}d\xi' P_a(\xi')$$
$$\times\left[\frac{\partial\left|G^R_{cc12}(\mathbf{r}_a,\mathbf{r}_b;\xi)\right|^2}{\partial(eV_b)}\int_0^{eV_b-\xi}d\xi'' P_b(\xi'') + \left|G^R_{cc12}(\mathbf{r}_a,\mathbf{r}_b;\xi)\right|^2 P_b(eV_b-\xi)\right]. \quad \text{(D1)}$$

The expression for $\mathcal{G}^{EC}_{ab}$ is obtained from the above formula by substitutions $eV_b \to -eV_b$, $G^R_{cc12} \to G^R_{cc11}$. The total nonlocal differential conductance is then given by

$$\mathcal{G}_{ab} = \mathcal{G}^{CAR}_{ab} + \mathcal{G}^{EC}_{ab}. \tag{D2}$$

The expressions for the full retarded and advanced Green's functions in the superconducting electrode are obtained from the system (7) and are given by

$$\begin{aligned}\hat{\mathbf{G}}^{R,A}_{cc}(\mathbf{x}_a,\mathbf{x}_b;\epsilon) = \big\{&\boldsymbol{\tau}_0 - \hat{\mathbf{g}}^{R,A}_{cc}(\mathbf{x}_a,\mathbf{x}_a;\epsilon)\hat{\boldsymbol{\Sigma}}^{R,A}_{ca}\hat{\mathbf{g}}^{R,A}_{\tilde{a}\tilde{a}}(\mathbf{x}_a,\mathbf{x}_a;\epsilon)\hat{\boldsymbol{\Sigma}}^{R,A}_{ac}\\
&-\hat{\mathbf{g}}^{R,A}_{cc}(\mathbf{x}_a,\mathbf{x}_b;\epsilon)\hat{\boldsymbol{\Sigma}}^{R,A}_{cb}\big[\boldsymbol{\tau}_0 - \hat{\mathbf{g}}^{R,A}_{\tilde{b}\tilde{b}}(\mathbf{x}_b,\mathbf{x}_b;\epsilon)\hat{\boldsymbol{\Sigma}}^{R,A}_{bc}\hat{\mathbf{g}}^{R,A}_{cc}(\mathbf{x}_b,\mathbf{x}_b;\epsilon)\hat{\boldsymbol{\Sigma}}^{R,A}_{cb}\big]^{-1}\\
&\times\hat{\mathbf{g}}^{R,A}_{\tilde{b}\tilde{b}}(\mathbf{x}_b,\mathbf{x}_b;\epsilon)\hat{\boldsymbol{\Sigma}}^{R,A}_{bc}\hat{\mathbf{g}}^{R,A}_{cc}(\mathbf{x}_b,\mathbf{x}_a;\epsilon)\hat{\boldsymbol{\Sigma}}^{R,A}_{ca}\hat{\mathbf{g}}^{R,A}_{\tilde{a}\tilde{a}}(\mathbf{x}_a,\mathbf{x}_a;\epsilon)\hat{\boldsymbol{\Sigma}}^{R,A}_{ac}\big\}^{-1}\\
&\times\big\{\hat{\mathbf{g}}^{R,A}_{cc}(\mathbf{x}_a,\mathbf{x}_b;\epsilon) + \hat{\mathbf{g}}^{R,A}_{cc}(\mathbf{x}_a,\mathbf{x}_b;\epsilon)\hat{\boldsymbol{\Sigma}}^{R,A}_{cb}\big[\boldsymbol{\tau}_0 - \hat{\mathbf{g}}^{R,A}_{\tilde{b}\tilde{b}}(\mathbf{x}_b,\mathbf{x}_b;\epsilon)\hat{\boldsymbol{\Sigma}}^{R,A}_{bc}\hat{\mathbf{g}}^{R,A}_{cc}(\mathbf{x}_b,\mathbf{x}_b;\epsilon)\hat{\boldsymbol{\Sigma}}^{R,A}_{cb}\big]^{-1}\\
&\times\hat{\mathbf{g}}^{R,A}_{\tilde{b}\tilde{b}}(\mathbf{x}_b,\mathbf{x}_b;\epsilon)\hat{\boldsymbol{\Sigma}}^{R,A}_{bc}\hat{\mathbf{g}}^{R,A}_{cc}(\mathbf{x}_b,\mathbf{x}_b;\epsilon)\big\}.\end{aligned} \tag{D3}$$

[1] P. Recher, E. V. Sukhorukov, and D. Loss, Phys. Rev. B **63**, 165314 (2001); L. Hofstetter, S. Csonka, J. Nygård, and C. Schönenberger, Nature (London) **461**, 960 (2009).

[2] P. Recher and D. Loss, Phys. Rev. B **65**, 165327 (2002); A. Schroer, B. Braunecker, A. L. Yeyati, and P. Recher, Phys. Rev. Lett. **113**, 266401 (2014).

[3] J. Cayssol, Phys. Rev. Lett. **100**, 147001 (2008); F. Crépin, H. Hettmansperger, P. Recher, and B. Trauzettel, Phys. Rev. B **87**, 195440 (2013).

[4] R. W. Reinthaler, P. Recher, and E. M. Hankiewicz, Phys. Rev. Lett. **110**, 226802 (2013); K. Sato and Y. Tserkovnyak, Phys. Rev. B **90**, 045419 (2014).

[5] J. Wang, L. Hao, and K. S. Chan, Phys. Rev. B **91**, 085415 (2015).

[6] S. Kawabata, J. Phys. Soc. Jpn. **70**, 1210 (2001); N. M. Chtchelkatchev, G. Blatter, G. B. Lesovik, and T. Martin, Phys. Rev. B **66**, 161320 (2002); A. Bednorz and W. Belzig, *ibid.* **83**, 125304 (2011); B. Braunecker, P. Burset, and A. L. Yeyati, Phys. Rev. Lett. **111**, 136806 (2013).

[7] P. Samuelsson, E. V. Sukhorukov, and M. Büttiker, Phys. Rev. Lett. **91**, 157002 (2003).

[8] W. Kłobus, A. Grudka, A. Baumgartner, D. Tomaszewski, C. Schönenberger, and J. Martinek, Phys. Rev. B **89**, 125404 (2014); H. Soller, L. Hofstetter, and D. Reeb, Europhys. Lett. **102**, 50009 (2013).

[9] G. Burkard and D. Loss, Phys. Rev. Lett. **91**, 087903 (2003).

[10] A. Cottet, T. Kontos, and A. L. Yeyati, Phys. Rev. Lett. **108**, 166803 (2012).

[11] Z. Scherübl, A. Pàlyi, and S. Csonka, Phys. Rev. B **89**, 205439 (2014).

[12] G. Falci, D. Feinberg, and F. W. J. Hekking, Europhys. Lett. **54**, 255 (2001).

[13] R. Mélin and D. Feinberg, Eur. Phys. J. B **26**, 101 (2002).

[14] D. Feinberg, Eur. Phys. J. B **36**, 419 (2003).

[15] P. Recher and D. Loss, Phys. Rev. Lett. **91**, 267003 (2003).

[16] D. Beckmann, H. B. Weber, and H. v. Löhneysen, Phys. Rev. Lett. **93**, 197003 (2004); S. Russo, M. Kroug, T. M. Klapwijk, and A. F. Morpurgo, *ibid.* **95**, 027002 (2005); P. Cadden-Zimansky and V. Chandrasekhar, *ibid.* **97**, 237003 (2006); A. Kleine, A. Baumgartner, J. Trbovic, and C. Schönenberger, Europhys. Lett. **87**, 27011 (2009); J. Wei and V. Chandrasekhar, Nat. Phys. **6**, 494 (2010).

[17] R. Mélin, C. Benjamin, and T. Martin, Phys. Rev. B **77**, 094512 (2008); M. S. Kalenkov and A. D. Zaikin, *ibid.* **75**, 172503 (2007); A. Freyn, M. Flöser, and R. Mélin, *ibid.* **82**, 014510 (2010); M. Flöser, D. Feinberg, and R. Mélin, *ibid.* **88**, 094517 (2013).

[18] R. Mélin, F. S. Bergeret, and A. L. Yeyati, Phys. Rev. B **79**, 104518 (2009).

[19] R. Mélin and D. Feinberg, Phys. Rev. B **70**, 174509 (2004).

[20] A. L. Yeyati, F. S. Bergeret, A. Martín-Rodero, and T. M. Klapwijk, Nat. Phys. **3**, 455 (2007).

[21] A. L. Yeyati, A. Martin-Rodero, D. Esteve, and C. Urbina, Phys. Rev. Lett. **87**, 046802 (2001).

[22] A. L. Yeyati, J. C. Cuevas, and A. Martín-Rodero, Phys. Rev. Lett. **95**, 056804 (2005).

[23] M. Kindermann and Yu. V. Nazarov, Phys. Rev. Lett. **91**, 136802 (2003).

[24] D. S. Golubev and A. D. Zaikin, Phys. Rev. B **82**, 134508 (2010).

[25] J. P. Pekola, J. J. Vartiainen, M. Möttönen, O.-P. Saira, M. Meschke, and D. V. Averin, Nat. Phys. **4**, 120 (2007); J. P. Pekola, V. F. Maisi, A. Kemppinen, M. Möttönen, Y. A. Pashkin, and D. V. Averin, Rev. Mod. Phys. **85**, 1421 (2013); D. M. T. van Zanten, D. M. Basko, I. M. Khaymovich, J. P. Pekola, H. Courtois, and C. B. Winkelmann, Phys. Rev. Lett. **116**, 166801 (2016).

[26] D. V. Averin and J. P. Pekola, Phys. Rev. Lett. **101**, 066801 (2008); T. Aref, V. F. Maisi, M. Gustafsson, P. Delsing, and J. P. Pekola, Europhys. Lett. **96**, 37008 (2011); S. V. Lotkhov, O.-P. Saira, J. P. Pekola, and A. B. Zorin, New J. Phys. **13**, 013040 (2011); V. Bubanja, J. Low Temp. Phys. **175**, 564 (2014); C.-H. Sun, P.-C. Tai, J.-A. Jiang, C.-S. Wu, J.-C. Chen, and Y.-F. Chen, Appl. Phys. Lett. **104**, 232601 (2014); A. Di Marco, V. F. Maisi, F. W. J. Hekking, and J. P. Pekola, Phys. Rev. B **92**, 094514 (2015).

[27] M. H. Devoret, D. Esteve, H. Grabert, G.-L. Ingold, H. Pothier, and C. Urbina, Phys. Rev. Lett. **64**, 1824 (1990).

[28] G. E. Blonder, M. Tinkham, and T. M. Klapwijk, Phys. Rev. B **25**, 4515 (1982).

[29] J. C. Cuevas, A. Martín-Rodero, and A. L. Yeyati, Phys. Rev. B **54**, 7366 (1996).
[30] F. W. J. Hekking and Yu. V. Nazarov, Phys. Rev. B **49**, 6847 (1994).
[31] V. Bubanja, Phys. Rev. B **83**, 195312 (2011).
[32] V. Bubanja and S. Iwabuchi, Phys. Rev. B **84**, 094501 (2011).
[33] G. Bignon, M. Houzet, F. Pistolesi, and F. W. J. Hekking, Europhys. Lett. **67**, 110 (2004).
[34] R. Mélin, Phys. Rev. B **73**, 174512 (2006).
[35] S. Duhot and R. Mélin, Phys. Rev. B **75**, 184531 (2007).
[36] D. S. Golubev, M. S. Kalenkov, and A. D. Zaikin, Phys. Rev. Lett. **103**, 067006 (2009).
[37] F. S. Bergeret and A. L. Yeyati, Phys. Rev. B **80**, 174508 (2009).
[38] F. Hübler, J. C. Lemyre, D. Beckmann, and H. v. Löhneysen, Phys. Rev. B **81**, 184524 (2010).
[39] V. Bubanja and S. Iwabuchi, Phys. Rev. B **79**, 035312 (2009).